

# Research on cable thermal characteristic detection technology based on the combination of support vector machine and thermal imaging technology

Ning Zhao<sup>1,\*</sup>, Kang Guo<sup>1</sup>, Qian Li<sup>1</sup>, Siying Wang<sup>1</sup>, Ziguang Zhang<sup>1</sup> and Lei Fan<sup>1</sup>

<sup>1</sup> State Grid Shijiazhuang Electric Power Supply Company, Shijiazhuang, Hebei, 050000, China

Corresponding authors: (e-mail: hbfy\_zn@163.com).

**Abstract** Timely detection and discovery of abnormal temperatures is the key to improving the service life of cables. In this paper, the thermal-force coupling field (temperature field and stress field) of cable joints is mathematically modeled to quantify cable energy changes. The infrared detection technology is used to measure the temperature of the cable and generate a thermogram to investigate the trend of the cable's thermal state. The machine learning algorithm "Support Vector Machine" (SVM) and Sparrow Search Algorithm (SSA) are integrated to identify the local thermal characteristics of cables from three aspects: feature extraction, parameter optimization and pattern recognition. Simulation experiments are conducted to test the quality of the proposed detection technique. The results show that when the cable has localized thermal aging, the frequency response of the channel in this part are less than 0dB, which can not transmit the signal normally, and need to be maintained in time. The technology in this paper can realize the effective detection of cable thermal characteristics and reduce the risk of cable faults.

**Index Terms** thermal-force coupled field, infrared temperature measurement, thermal imaging, SSA-SVM, cable thermal characteristics

## I. Introduction

Distribution line overheating defects refers to a series of problems caused by distribution lines in the process of operation, due to the current exceeding the rated current carrying capacity of the cable or the high temperature of the cable-laying environment, resulting in an increase in the temperature of the cable and its surrounding environment [1]. Overheating defects in distribution lines are one of the common faults in power systems, which can have a serious impact on the safe and stable operation of power grids [2]. Firstly, when cables run under overheating for a long period of time, it will accelerate the aging of cables and thus shorten the service life of cables, and at the same time, it will increase the maintenance and overhaul cost of the lines [3], [4]. Secondly, overheating of distribution lines may lead to problems such as cable breakage and joint failure, thus affecting the stability of power supply [5], [6]. Not only that, overheating of cables can also lead to deformation, cracking, and even burning of the outer sheath of cables, which can lead to fire accidents, and the fire will not only cause property loss, but also may threaten the safety of people's lives [7], [8]. Based on this, effective measures should be taken to prevent and manage the defects in order to ensure the stability and safety of power grid operation through timely detection and elimination of defects [9].

Infrared radiation is the most widespread radiation in nature, and the energy of infrared radiation is directly related to the temperature of the surface of the object, and the use of this property can be achieved without contacting the object to measure the surface temperature of the object [10]. Among them, overhead distribution lines are exposed and visible, which is the most widely used place for infrared thermography. Using infrared thermography, the temperature of various parts of the distribution line, such as connection points, contacts, knife gates, etc., can be easily measured on the ground to quickly find overheating defects. If the measured equipment as a whole is overheated, it can be initially judged to be caused by overload [11]-[13]. If only individual points are overheated, it can be judged as a local resistance increase due to poor contact or oxidation [14], [15]. With the development of power operation and maintenance technology, further combined with intelligent decision-making modeling to improve the defect diagnosis ability of cable thermal imaging detection technology, and then timely find out the hidden defects of distribution lines and solve them, to protect the reliable operation of the power grid [16]-[18].

In this paper, the temperature and stress fields of cable joints are mathematically modeled to focus on the thermal coupling of cables by means of quantitative analysis. An infrared detection instrument is used to accept the infrared radiant energy when the cable is running, and the corresponding thermal image is generated to visualize the details

of the heat distribution on the cable surface. Several statistical characteristic parameters are selected to describe the local heating spectra, and the SSA-SVM model is constructed to realize parameter optimization, identify the cable heating pattern and locate the fault point. Conduct cable terminal simulation experiments. Analyze the temperature distribution of localized heat generation and its influence on the maximum temperature of the cable, etc., identify the transmission characteristics of localized heat aging cables, and verify the practical application value of the detection technology at the same time.

## II. Analysis of cable thermal characteristic detection technology based on vector machine

This chapter systematically analyzes how cable thermal characterization can be achieved through techniques such as infrared detection thermal imagers and vector machine models.

### II. A. Mathematical model of thermal-force coupling field of cable gland

#### II. A. 1) Mathematical Modeling of Temperature Field

For the problem of analyzing the temperature field of a cable joint, according to Fourier's law of heat transfer and the law of conservation of energy, the governing equations describing the temperature field problem can be obtained, which can be written in the right-angled coordinate system as:

$$\rho c \frac{\partial T}{\partial t} - \frac{\partial}{\partial x} (\lambda_x \frac{\partial T}{\partial x}) - \frac{\partial}{\partial y} (\lambda_y \frac{\partial T}{\partial y}) - \frac{\partial}{\partial z} (\lambda_z \frac{\partial T}{\partial z}) - Q_v = 0 \quad (1)$$

where  $\rho$  is the density of the material;  $c$  is the specific heat capacity of the material;  $T$  is the temperature variable to be solved;  $t$  is the time;  $\lambda_x, \lambda_y$  and  $\lambda_z$  are the thermal conductivities of the material along the direction of  $x, y$  and  $z$ , respectively, and for a homogeneous material there is  $\lambda_x = \lambda_y = \lambda_z$ ;  $Q_v$  is the heat generated per unit volume inside the object, i.e., the heat source density.

Equation (1) is also known as the heat balance equation, i.e., the amount of heat required to increase the temperature of an object should be equal to the sum of the heat transferred from the outside into the interior of the object and the heat produced by the heat source inside the object. Among them, the first term for the unit of time required to increase the temperature of the heat; the second, third and fourth term for the outside world by  $x, y$  and  $z$  direction into the object's internal heat; the fifth term for the object's internal heat generated by the unit volume.

Temperature field solution problem common boundary conditions are divided into the following three categories:

(1) The first type of boundary conditions is given the value of the temperature on the boundary, the expression is:

$$T|_{\Gamma_1} = T_0 \quad (2)$$

(2) The second type of boundary condition is given the normal heat flow density on the boundary with the expression:

$$-\lambda \frac{\partial T}{\partial n} |_{\Gamma_2} = q_2 \quad (3)$$

(3) The third type of boundary conditions is given the temperature of the surroundings and the convective heat transfer coefficient between the surface of the object and the surroundings, expressed as:

$$-\lambda \frac{\partial T}{\partial n} |_{\Gamma_3} = h(T_f - T_{amb}) \quad (4)$$

where  $h$  is the surface convection heat transfer coefficient;  $T_f$  is the surface temperature of the heat generator;  $T_{amb}$  is the ambient temperature.

In addition, for cable glands laid in air, there is also radiative heat dissipation between its surface and the surrounding environment.

According to Stephen Boltzmann's law, the radiative heat dissipation boundary on the cable surface can be expressed as:

$$-\lambda \frac{\partial T}{\partial n} = \sigma_0 \varepsilon (T_f^4 - T_{amb}^4) \quad (5)$$

where  $\sigma_0 = 5.66 \times 10^{-8}$  is the Stephen Boltzmann constant,  $W/(m^2 \cdot K^4)$ ; and  $\varepsilon$  is the surface emissivity.

## II. A. 2) Mathematical modeling of the stress field

Since the cable shield is very thin, in order to simplify the calculation, the stress changes caused by electromagnetic forces can be ignored. The analysis of the thermal stress field problem satisfied by the structure of power cable joints can also be described by a series of tensor forms of the system of equations as follows:

$$\begin{cases}
 \frac{\partial \sigma_{ij}}{\partial x_j} + f_i = \rho \frac{\partial^2 u_i}{\partial t^2} + \mu \frac{\partial u_i}{\partial t} & \text{(a)} \\
 \varepsilon_{ij} = \frac{1}{2} \left( \frac{\partial u_i}{\partial x_j} + \frac{\partial u_j}{\partial x_i} \right) & \text{(b)} \\
 \varepsilon_{ij} = \varepsilon_{ij}^E + \varepsilon_{ij}^{Th} & \text{(c)} \\
 \sigma_{ij} = D_{ijkl} \varepsilon_{kl}^E & \text{(d)} \\
 \varepsilon_{ij}^{Th} = \alpha \Delta T \delta_{ij} & \text{(e)} \\
 u_i |_{\Gamma_s} = \bar{u}_i & \text{(f)} \\
 \sigma_{ij} n_j |_{\Gamma_\sigma} = \bar{\sigma}_{ij} & \text{(g)}
 \end{cases} \quad (6)$$

where  $\sigma$  is the stress tensor;  $f$  is the externally applied force;  $\rho$  is the material density;  $u$  is the displacement;  $t$  is the time;  $\mu$  is the damping coefficient;  $\varepsilon$  is the strain tensor;  $\varepsilon^E$  is the elastic strain component;  $\varepsilon^{Th}$  is the thermal strain component;  $D$  is the strain coefficient;  $\alpha$  is the coefficient of linear expansion;  $\Delta T$  is the amount of temperature change compared to the reference temperature;  $\bar{u}_i$  is the value of displacement on the boundary; and  $\bar{\sigma}_{ij}$  is the value of stress on the boundary. Also,  $i = j = k = l = 1, 2, 3, 4$ .

where the fourth order tensor  $D$  can be determined by the following equation:

$$D_{ijkl} = \frac{E(T)}{1+\nu} \delta_{ik} \delta_{jl} + \frac{E(T)}{(1+\nu)(1-2\nu)} \delta_{ij} \delta_{kl} \quad (7)$$

where  $E(T)$  is the Young's modulus of the material;  $\nu$  is the Poisson's ratio of the material; and  $\delta_{ij}$  is the Clark's function, the expression of which is shown below:

$$\delta_{ij} = \begin{cases} 1, & i = j \\ 0, & i \neq j \end{cases} \quad (8)$$

Bringing Eq. (6(e)) into Eq. (6(c)) gives:

$$\varepsilon_{ij} = \varepsilon_{ij}^E + \alpha \Delta T \delta_{ij} \quad (9)$$

Combined with Eq. (6(b)) yields:

$$\varepsilon_{ij}^E = \frac{1}{3} \left( \frac{\partial u_i}{\partial x_j} + \frac{\partial u_j}{\partial x_i} \right) - \alpha \Delta T \delta_{ij} \quad (10)$$

Bringing Eq. (6) into Eq. (6(d)), the stress expression can be derived as:

$$\sigma_{ij} = \frac{1}{3} D_{ijkl} (u_{k,l} + u_{l,k}) - \alpha(T) \Delta T D_{ijkl} \delta_{kl} \quad (11)$$

## II. B. Principles of detection technology

### II. B. 1) Infrared Detection Fundamentals

Any object as long as its temperature is higher than absolute zero ( $-274^\circ \text{C}$ ), due to the movement of its own molecules, it will continue to emit thermal radiation to the outside, the object temperature is different, the energy radiated is different, and the wavelength of the radiation wave is also different. According to Stefan-Boltzmann law, the energy radiated by the object is:

$$Q = \sigma \varepsilon T^4 \quad (12)$$

where  $\sigma$  - Steven Bozeman's constant;  $\varepsilon$  - is the surface emissivity of the object;  $T$  - the the absolute temperature of the surface of the object. Infrared thermal imager through the reception of infrared radiation energy emitted by the object, the infrared detector will be the power of the object radiation signal converted into electrical signals, the output signal of the imaging device can be exactly one-to-one correspondence to simulate the spatial distribution of the temperature of the surface of the scanned object; processed by the electronic system, transmitted to the display, and the surface of the object to get the thermal distribution of thermal distribution of heat corresponding to the thermal image, so as to accurately determine the distribution of temperature on the surface of the object.

There are many similarities between a running equipment and a human body. The vast majority of equipment failures are related to local or overall overheating or abnormal temperature distribution. When the parts of the equipment failure, whether it is wear and tear, fatigue, rupture, deformation, corrosion, peeling, leakage, clogging, loosening, melting, material deterioration, contamination and abnormal vibration, etc., the vast majority of this phenomenon are directly or indirectly related to the change in its temperature.

Equipment failure, its overall or local thermal balance to be damaged or affected, through the heat of the various modes of propagation, the heat inside the equipment must gradually reach its external surface, resulting in changes in the temperature field of the external surface.

The use of infrared detection equipment to capture the information of these infrared radiation, through quantitative analysis of the detection results can be determined by the nature of the failure of the equipment, parts and degree, and then predict the development trend of the failure and the life of the equipment.

## II. B. 2) Cable infrared detection and diagnosis methods

At present, the basic method of infrared detection is divided into two major types of active and passive, and the most widely used in marine cable fault diagnosis for passive detection. Cable infrared detection of the work content based on the actual project needs, mainly the following kinds:

(1) Daily inspection, daily inspection is carried out by the operator or infrared personnel, the application of simple or portable infrared detector, infrared temperature measurement of the key parts of the cable, and record storage.

(2) regular testing, according to the importance of various marine cable size and new and old degree of development of a comprehensive testing cycle, to use infrared thermal imaging equipment to run the cable for detailed and comprehensive infrared detection, record keeping.

(3) Focus on tracking, in the daily inspection and regular testing on the basis of the cable found to have overheating suspects to talk about focusing on tracking and testing, the situation is more serious to continuous tracking and testing, record and inventory, watch the development trend.

(4) With the overhaul, when the ship is ready to overhaul, infrared detection should be carried out with the overhaul work. Can be planned before the repair test to confirm the performance of various types of cables, overhaul goals and directions; can also be carried out after the repair to test the effect of repair and quality.

(5) basic testing, for the new ship, to be put into operation to enter a stable state (especially after the thermal stability of the state, in order to grasp the performance of its cables, infrared detection, recording and storage of the disk, as the ship's cable equipment for the infrared infrared base information for the future analysis of faults and defects and prediction of the life of the basis for laying the foundation.

The above describes several ways of infrared detection of marine cables. Detection of the ultimate goal of the cable technology state diagnosis. At present, the use of infrared monitoring technology to diagnose electrical equipment faults are mainly the following methods;

(1) Surface absolute temperature judgment method: according to the infrared thermometer measured surface temperature of the cable, with reference to the limit value of the maximum permissible temperature of heat generation of each part of the national standard, the state of its judgment.

(2) Relative temperature difference method: the relative temperature difference refers to the equipment condition is the same or basically the same (refers to the equipment type, installation location, ambient temperature, surface condition and load current, etc.) of the temperature difference between the two corresponding measurement points, and which the hotter measurement point temperature rise of the ratio of the mathematical expression for:

$$\delta_t = \frac{\tau_1 - \tau_2}{\tau_1} \times 100\% = \frac{T_1 - T_2}{T_1 - T_0} \times 100\% \quad (13)$$

where,  $\tau_1$  and  $T_1$  - the temperature rise and temperature at the point of heat generation,  $\tau_2$  and  $T_2$  - the temperature rise and temperature of the normal corresponding point,  $T_0$  - temperature of the ambient reference body.

Relative temperature difference judgment method is proposed in order to exclude the influence of different loads of equipment and different temperatures of bad environment on the results of infrared detection and diagnosis. When the ambient temperature is low, especially the load current is small, the temperature value of the equipment does not exceed the normative standards, but a large number of facts prove that the temperature value at this time does not indicate that the equipment does not have defects or faults exist, often after the load growth, or the ambient temperature rises, it will cause equipment accidents.

(3) The same type (same phase) comparison method: refers to the same type of equipment being tested for comparison. Specific practice is to compare the corresponding part of the temperature value of similar equipment, so that it is easier to determine whether the equipment is normal. In the same kind of comparison, we must pay attention to not exclude the possibility of their simultaneous existence of thermal faults.

(4) Thermal spectrum analysis: is based on similar equipment in the normal state and abnormal state of the difference between the thermal spectrum to determine whether the equipment is normal method.

(5) File analysis method: also known as the historical data comparison method, is the measurement results with the equipment of infrared diagnostic technology file compared to analyze the diagnostic method. This method is conducive to the important, complex structure of the equipment for the correct diagnosis. Application of this method is the premise of the equipment to be diagnosed to establish infrared diagnostic technology files, so that in the diagnosis, you can analyze the equipment in different periods of infrared detection results, including temperature, temperature rise and temperature field distribution changes, to grasp the trend of the thermal state of the equipment, and should also be referred to the other relevant test results in order to comprehensively analyze and make judgments.

## II. C. Support vector machine principle analysis

Support vector machine is a commonly used machine learning algorithm whose core idea is to divide spatial features into two parts by finding a hyperplane with maximum geometric spacing. In linearly divisible support vector machines, the sample data can be perfectly divided into two classes, so a hyperplane can be found to separate them completely. Whereas in linear support vector machines, due to some noise and overlap between the data, a better classification result is needed by introducing a soft interval to allow for some misclassification. Finally, in nonlinear support vector machines, since the data distribution presents a nonlinear structure, it is necessary to map the data to a high dimensional space by using a kernel function before finding an optimal division hyperplane.

### II. C. 1) Sparrow Search Algorithm

The Sparrow Search Approach (SSA) is a new population intelligence algorithm evolved from the foraging and anti-predation behavior of sparrows, which is simple and efficient and can achieve global convergence. According to the mathematical model of the algorithm, the population composed of foraging sparrows can be represented by equation (14):

$$X = \begin{bmatrix} X_1 \\ X_2 \\ \vdots \\ X_n \end{bmatrix} = \begin{bmatrix} x_{1,1} & x_{1,2} & \cdots & x_{1,d} \\ x_{2,1} & x_{2,2} & \cdots & x_{2,d} \\ \vdots & \vdots & \vdots & \vdots \\ x_{n,1} & x_{n,2} & \cdots & x_{n,d} \end{bmatrix} \quad (14)$$

where  $d$  denotes the dimension of the problem to be optimized,  $n$  denotes the number of sparrows, and  $x_{i,j}$  is the position of the  $i$  th sparrow in the  $j$  th dimension. The value of sparrow population fitness is shown in vector equation (15):

$$F_x = \begin{bmatrix} f(x_{1,1}, x_{1,2}, \dots, x_{1,d}) \\ f(x_{2,1}, x_{2,2}, \dots, x_{2,d}) \\ \vdots \\ f(x_{n,1}, x_{n,2}, \dots, x_{n,d}) \end{bmatrix} \quad (15)$$

where each row of  $F_x$  represents the fitness value of the individual sparrow.

Given that the finder is responsible for finding food and guiding the moving direction of the whole sparrow population in the sparrow population during the foraging process, it has a better fitness value than other sparrow individuals and is able to prioritize access to food. Therefore, the position of the finder can be updated by equation (16) during the delivery of generations:

$$X_i^{t+1} = \begin{cases} X_i^t \cdot e^{-\frac{i}{\alpha \cdot t_{\max}}} & \text{if } V_a < V_s \\ X_i^t + r_d \cdot U & \text{if } V_a \geq V_s \end{cases} \quad (16)$$

where  $X_i^t$  denotes the position of the  $i$ th finder after the  $t$ th iteration,  $t_{\max}$  denotes the maximum number of iterations, and  $t$  denotes the current number of iterations.  $\alpha \in (0,1]$  is a random number,  $r_d$  is a random number obeying a normal distribution, and  $U \in \mathbb{R}^{1 \times d}$  is the unit matrix.  $V_a \in [0,1]$  is the warning value and  $V_s \in [0.55,1]$  is the safety threshold. When  $V_a < V_s$ , it means that no predator is found in the sparrow population and the finder can continue to expand the foraging range; when  $V_a \geq V_s$ , it means that a predator is found in the population, and all the sparrows move to the safe area quickly.

During the foraging process, the joiner will always monitor the finder. As soon as the discoverer finds a better food, they go to fight for it. According to this rule, the joiner position movement formula is:

$$X_i^{t+1} = \begin{cases} r_d \cdot e^{(X_{\text{wst}} - X_i^t)/t^2} & \text{if } i > n/2 \\ X_{\text{op}}^{t+1} + \|X_i^t - X_{\text{op}}^{t+1}\| \cdot A^+ \cdot U & \text{others} \end{cases} \quad (17)$$

where  $X_{\text{op}}$  is the current optimal position of the discoverer and  $X_{\text{wst}}$  denotes the global worst position. The element values of  $A \in \mathbb{R}^{1 \times d}$  are all 1 or -1, and  $A^+ = A^T(AA^T)^{-1}$ . When  $i > n/2$ , it means that the  $i$ th accession has a worse fitness value.

Vigilantes account for 15% to 25% of the total population size and the initial positions of the vigilantes are randomly generated in the population.

According to the algorithm rules, the vigilant movement position can be calculated by equation (18):

$$X_i^{t+1} = \begin{cases} X_{\text{bst}}^t + \beta \cdot \|X_i^t - X_{\text{bst}}^t\| & \text{if } f_i > f_b \\ X_i^t + r \cdot (\|X_i^t - X_{\text{bst}}^t\| / ((f_i - f_w) + \varepsilon)) & \text{if } f_i = f_b \end{cases} \quad (18)$$

where  $X_{\text{bst}}$  is the current global optimal position,  $\beta$  is the step control parameter, and  $r \in [-1,1]$  is a random number;  $f_i$  is the current fitness value of the individual sparrow, and  $f_b$  and  $f_w$  are the current global optimal and worst fitness values, respectively;  $\varepsilon$  is the conditioning factor.

## II. C. 2) SSA-SVM based cable thermal identification

### (1) Cable thermal feature vector extraction

The cable localized heat generation PRPD feature spectrogram describes the relationship between the number of heat generation signals with different peaks and the phase angle. Since the PRPD spectrograms of different defects have different distribution characteristics, this paper selects several statistical feature parameters to describe the localized heat generation spectrograms.

Based on the calculation of the statistical feature parameters, the skewness  $Sk$ , mean value  $\mu$ , standard deviation  $\sigma$ , steepness  $Ku$ , heat factor  $Q$ , correlation number  $cc$ , and phase asymmetry  $\Phi$  are extracted as the statistical features to characterize the differences in the heat generation types of each type of defects, respectively.

The skewness  $Sk$  reflects the degree of skewness of the distribution away from the symmetric distribution, and the steepness  $Ku$  reflects the sharpness or kurtosis of the distribution curve at the peak. Their formulas are shown in (19) and (20):

$$Sk = \sum_{i=1}^W (x_i - \mu)^3 p_i \Delta x / \sigma^3 \quad (19)$$

$$Ku = \left[ \sum_{i=1}^W (x_i - \mu)^4 p_i \Delta x / \sigma^4 \right] - 2 \quad (20)$$

where  $\Delta x$  is the width of the phase window,  $x_i$  is the phase of the  $i$  th phase window,  $W$  denotes the number of phase windows in half an IF cycle, and  $p_i, \mu$  and  $\sigma$  denote the probability, the mean, and the standard deviation of the events in the  $i$  th phase window, respectively. Where the expressions for  $p_i, \mu$  and  $\sigma$  are shown in Eqs. (21), (22) and (23):

$$p_i = \frac{y_i}{\sum_{i=1}^W y_i} \quad (21)$$

$$\mu = \sum_{i=1}^W \varphi_i p_i \quad (22)$$

$$\sigma = \sqrt{\sum_{i=1}^W p_i (x_i - \mu)^2} \quad (23)$$

In equation (21),  $y_i$  is the vertical coordinate of the  $\varphi-q$  plane.

The heat generation factor  $Q$  is a reflection of the difference in the average heat generation during the positive and negative half-weeks and is calculated as shown in Eq. (24):

$$Q = \frac{\sum_{i=1}^W n_i^- q_i^-}{\sum_{i=1}^W n_i^-} / \frac{\sum_{i=1}^W n_i^+ q_i^+}{\sum_{i=1}^W n_i^+} \quad (24)$$

In Eq. (24):  $n_i^+, n_i^-$  denotes the heating repetition rate in phase window  $i$ , and the superscripts “+” and “-” denote the positive and negative half-periods of the spectrograms of  $\varphi-q$ .

The correlation number  $cc$  reflects the shape similarity of the spectrograms in the positive and negative half-periods and is calculated as shown in equation (25):

$$cc = \frac{\sum q_i^+ q_i^- - \sum q_i^+ \sum q_i^- / n}{\sqrt{[\sum (q_i^+)^2 - (\sum q_i^+)^2 / n] \cdot [\sum (q_i^-)^2 - (\sum q_i^-)^2 / n]}} \quad (25)$$

In Eq. (25):  $q_i^+, q_i^-$  denotes the average heat generation within phase window  $i$ .

The phase asymmetry degree  $\Phi$  reflects the difference in the onset phases of heat generation within the positive and negative half-weeks of the  $\varphi-q$  spectra. The calculation formula is shown in equation (26):

$$\Phi = \varphi_{in}^- / \varphi_{in}^+ \quad (26)$$

In Eq. (26):  $\varphi_{in}^+, \varphi_{in}^-$  are the onset phase angles of the heat generation in the positive and negative half weeks of the  $\varphi-q$  spectrogram, respectively.

(2) Cable heat identification method based on SSA-SVM modeling

Figure 1 shows the steps of local heat pattern recognition of cable based on SSA optimization SVM model, which can be divided into three parts in general: feature extraction, parameter optimization and pattern recognition.

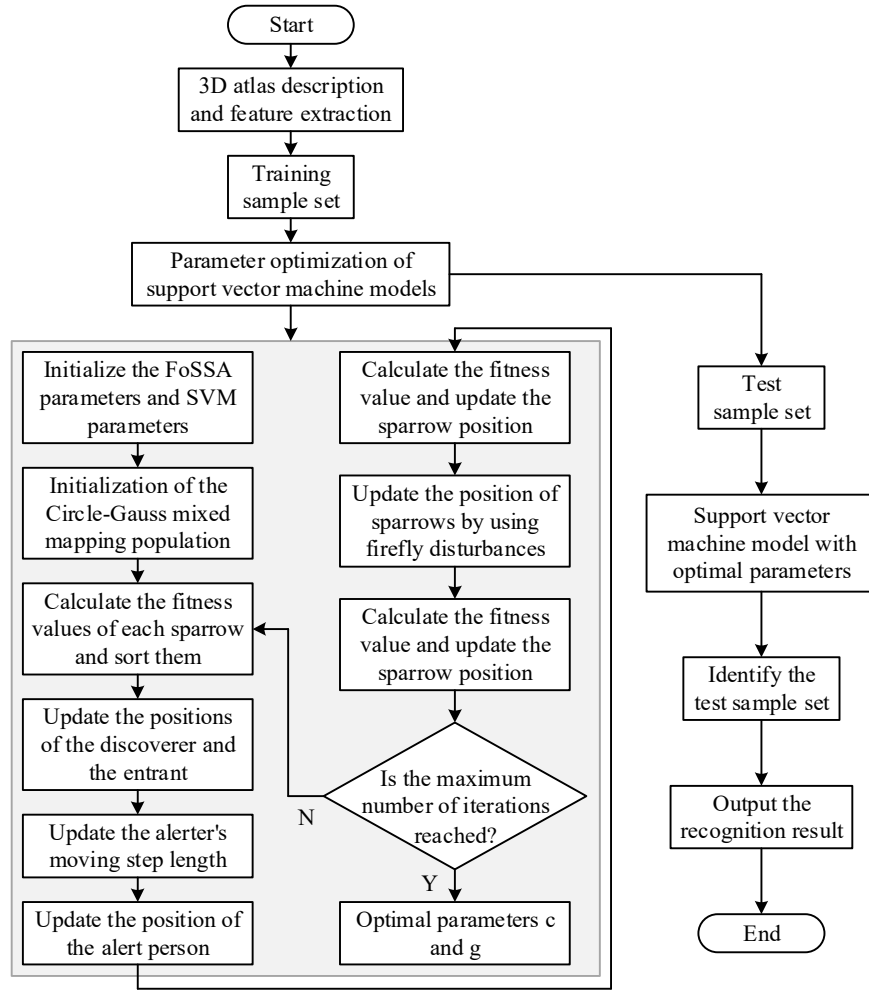


Figure 1: Partial discharge identification algorithm process of SSA optimized SVM

(1) Collect the thermal data of four types of insulation defective cables, draw 3D feature spectra, and extract key feature vectors by statistical feature parameters.

(2) Initialize SSA and SVM parameters, take the range of values of penalty factor  $c$  and kernel function parameter  $g$  as the search range of sparrow, and adopt Circle-Gauss hybrid mapping model to generate initial population.

(3) Use SSA algorithm for parameter optimization, use the error rate of pattern recognition in the training set in the sample as the objective function for iterative computation, get the optimal parameter combination  $(c, g)$  imported into the SVM model, and validate it with the test set. The steps of SSA to optimize the combination of parameters are:

Step1: Initialize the number of populations, number of iterations, proportion of discoverers and joiners, step control parameters, and  $c$  and  $g$ ;

Step2: Generate the initial population of sparrows using the Circle-Gauss hybrid mapping model;

Step3: calculating and ranking the fitness values.

Step4: update the discoverer and joiner positions according to equations (16) and (17);

Step5: Calculate the movement step length of the vigilant;

Step6: update the vigilant position according to equation (18);

Step7: update the firefly disturbed sparrow position;

Step8: calculate the adaptation value and update the sparrow position;

Step9: whether the stop condition is satisfied, if it is satisfied, exit and output the result, otherwise, repeat the execution of Step3-8.

### III. Cable thermal characteristics testing and results analysis

In this chapter, through simulation experiments, we study the temperature distribution and thermal characteristics of cables during localized thermal aging, etc., to verify the effectiveness of the detection technology in this paper.

#### III. A. Cable termination simulation experiment

##### III. A. 1) Cable termination simulation parameters

In order to verify the reliability of the cable thermal characteristic detection technology in this paper, this paper takes 120kV high-temperature oil-filled composite marine cable terminal as an example, and establishes the simulation model of its steady state thermal field by using finite element analysis method. The height of the terminal casing is 1.8m, the conductor current is set to 1200A, and Table 1 shows the radial dimensions of the cable terminal and the thermal conductivity of the main materials. The radii of the eight structures/parts of the cable terminal are determined according to the characteristics of the place, for example, the radius of the copper conductor is smaller, which is taken as 18.0/mm, and the thermal conductivity is  $385.50\text{W}\cdot(\text{m}\cdot\text{K})^{-1}$  to ensure that the parameters of the simulation experiments are in line with the actual cable operation and to avoid experimental errors.

Table 1: Simulation parameters of cable terminal

Serial number	Structure/part	Radius/mm	Thermal conductivity $/(W\cdot(m\cdot K)^{-1})$
1	Copper conductor	18.0	385.50
2	XLPE insulation	32.5	0.28
3	Stress cone/Reinforced insulation	-	0.29
4	Air	92.5	0.03
5	Silicone oil	92.5	0.17
6	Ring gas casing	137.5	0.33
7	Silicone rubber sheath	-	0.28
8	Pressure equalizing hood	192.5	80.50

##### III. A. 2) Cable termination surface temperature distribution

The temperature of the cable terminal surface is measured using an infrared detector. Taking the relative position of the height of the cable terminal as the X-axis and the temperature value of the terminal surface as the Y-axis, the temperature distribution of different positions of the cable terminal surface is obtained. Figure 2 shows the temperature distribution at different locations on the cable terminal surface. As can be seen from the figure, the temperature of the terminal surface shows a gradual decrease with the change of position, from  $29.28^{\circ}\text{C}$  at the initial position to  $25.73^{\circ}\text{C}$  at the final position. The analysis interval is 0.15m, and the average temperature of the terminal surface in different areas is calculated statistically, and the temperature difference value (the temperature difference value is taken as the difference between the temperature of the silicone oil layer and the temperature of the air layer) is calculated at the same time, and it can be seen that the corresponding average temperature of the terminal surface of the air layer is lower than that of the silicone oil layer by about  $0.7^{\circ}\text{C}$ , which is in line with the theoretical analysis results, indicating that the simulation model established is more in line with the actual situation.

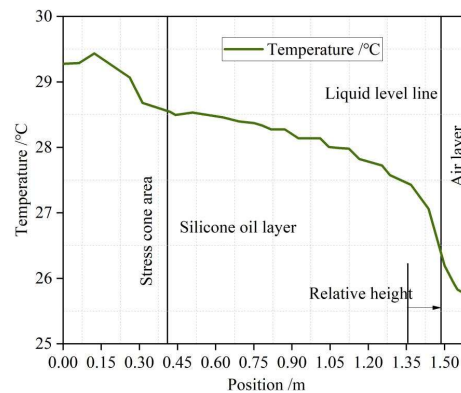


Figure 2: Temperature distribution of different areas on the terminal

##### III. A. 3) Relationship between terminal fluid and surface temperature distribution

The surface temperature distribution of the terminal at different silicone oil levels is given in Fig. 3. As the silicone oil level decreases, the temperature distribution range of the air layer of the terminal gradually expands from the

release range of 29-30°C to the distribution range of 26-30°C. And according to the local enlarged diagram of the temperature curve (the light green part in the middle), it can be seen that the surface temperature of the terminal corresponding to the silicone oil layer rises gradually with the decrease of the liquid level instead, which indicates that the degree of oil leakage of the terminal directly affects its overall heat dissipation efficiency, and the more serious the degree of oil leakage is, the worse the heat dissipation effect is. At the same time, the trend of the temperature difference between the terminal surface corresponding to the upper and lower regions of the liquid level at different levels was analyzed, and the analysis intervals  $\Delta h$  were taken as 0.05, 0.15, 0.25, and 0.35 m, respectively. As the terminal level height decreases, the temperature difference between the terminal surface corresponding to the upper and lower regions of the liquid level gradually expands, and the maximum temperature difference reaches about 2.19°C when the liquid level height decreases to 1.05m.

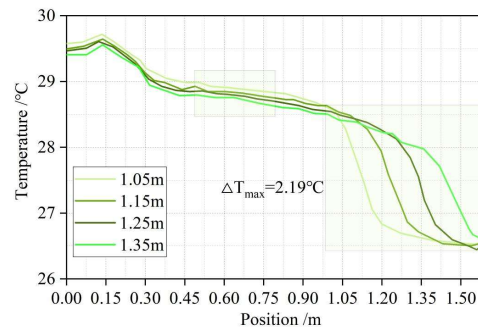


Figure 3: Relationship between liquid level and temperature distribution

### III. B. Thermal characterization of cables

#### III. B. 1) Thermal characterization of local hot spots

In the high-temperature oil-filled composite marine cable normal current-carrying work, its high-temperature superconducting strips may be due to manufacturing unevenness, fatigue loss resulting from long-time work, etc., part of the destruction of the oil leakage and lead to part of the loss of super (temperature exceeds the critical value, resulting in the cable to lose superconducting properties and transformed into a normally conductive state of the phenomenon), thus generating random localized hotspots. The hot spots generated in the strip cause localized temperature gradients, which propagate through the cable, generating heat and leading to system failure. Partial loss of excess can be subdivided into single strip loss of excess, single conductive layer loss of excess, and superconducting cable loss of excess. The first two states do not cause the cable air layer to heat up during steady state when considering engineering margins. Therefore, the thermal characteristics of the local hot spot cable are analyzed by setting up a fixed-type triple hot spot. Two 3-cm-long volumetric elements are arranged at 25m and 45m away from the liquid nitrogen inlet, respectively, and a constant heat is applied to them, and the mass flow rate of the LN2 inlet is set to be 0.10 kg/s for the steady-state and transient state studies. The thermal characteristics of the high-temperature oil-filled composite marine cable under the localized hot spot condition are simulated.

Figure 4 shows the steady state axial temperature distribution of the cable strip under the localized hot spot condition. The strip temperature of the high-temperature oil-filled composite marine cable increases with the increase of the cable length, and the temperature of the cable strip increases from 65.04°C to 65.43°C when the cable length increases from 0 to 60 m. The temperature of the cable strip increases with the increase of the cable length, and the temperature of the cable strip increases with the increase of the cable length. When the strip produces a localized hot spot, the strip temperature increases at that place, for example, a localized hot spot is produced at 25m and 45m, and the strip temperature appears to increase by a larger amount than the rest of the length. And as the localized heat increases, the strip temperature at the localized hotspot will continue to increase. It can be expected that when the localized hotspot exceeds a certain critical value, the strip loses its superexcursion at that location. It is interesting to note that the strip front end temperature does not change as the strip generates hot spots. In the region between the two hot spots of the strip, the strip temperature change trend is consistent with the change without hot spots. Therefore, in engineering applications, for cable fault detection, you can check the temperature of the cable strip with the length of the direction of the temperature, for the temperature rise area, timely maintenance of the cable to reduce the cable due to local hotspot hazards.

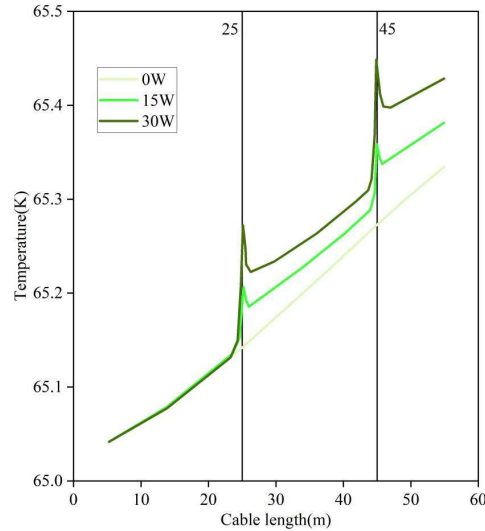


Figure 4: Steady-state axial temperature of cable strips under local hotspots

**III. B. 2) Influence of terminal heat leakage heat load on maximum cable temperature**

Thermal leakage at the terminals is the main reason for the increase in the temperature of the cable strip, and analyzing the effect of the variation of the thermal load with mass flow rate on the maximum temperature of the cable strip can be further explored as a necessity to reduce the losses caused by thermal leakage at the terminals to the cable system. Figure 5 shows the effect of the change of terminal heat load with mass flow rate on the maximum temperature of the cable strip. When the terminal heat load increases, the maximum temperature of the cable strip rises. As the mass flow rate increases from 0.01 kg/s to 0.16 kg/s, the maximum temperature of the cable strip first decreases sharply from about 73°C to about 66°C, and then slowly tends to a stabilized value of 65°C.

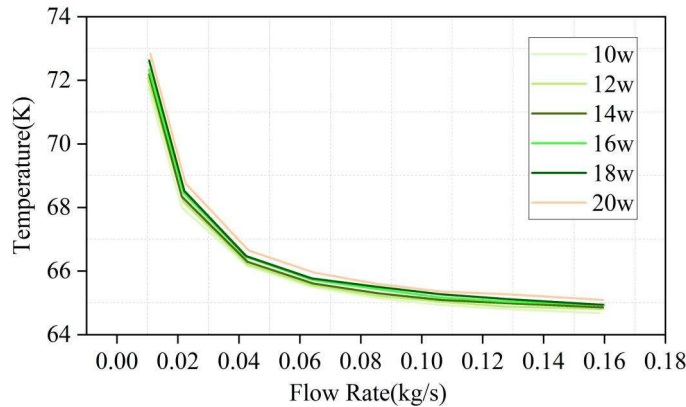


Figure 5: Influence of heat load variation on the maximum temperature

**III. B. 3) Cable coolant thermal entropy production rate distribution**

Figure 6 shows the distribution of thermal entropy production rate of cable coolant. Thermal entropy production has a maximum value at the corrugated wall surface of the cable. At the wall surface, the wall is in direct contact with the superconducting strip, and the heat generated by the high temperature superconducting strip is conducted along the wall to the center region. Therefore, there is a large temperature gradient at the wall surface, which results in a large thermal entropy production. As the heat is transferred to the center region, the temperature becomes lower and lower, and the distribution is more uniform, so that the thermal entropy yield in the center region is almost 0. From Fig. 6, it can be seen that the thermal gradient entropy yields are 0.05171, 0.04878, 0.04614, and 0.03983 when the mass flow rate of the coolant is 14, 16, 18, 20, and 22 L/min at  $Z=1m$ , respectively, 0.03645  $W/m^3K$ ; when  $Z=1.5m$ , the thermal gradient entropy production rate is 0.02733, 0.02676, 0.02613, 0.02576, 0.02525  $W/m^3K$ , respectively, and the thermal entropy production rate decreases with the increase of the mass flow rate of coolant. The reason for this was analyzed and found to be that the increase in mass flow rate decreases the coolant temperature, which leads to a decrease in the rate of thermal entropy generation.

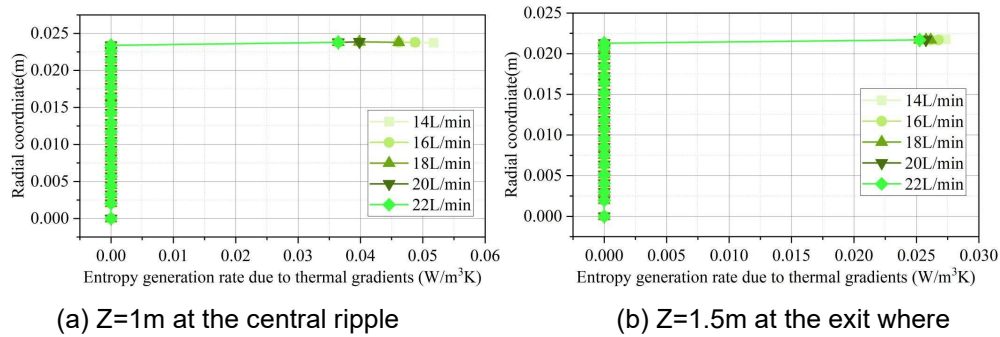


Figure 6: The generation rate distribution of thermal entropy of cable coolant

### III. B. 4) Transmission characteristics of localized thermally aged cables

According to the analytically obtained cable thermal characteristics can be further investigated the transmission characteristics of localized heat aging cables. Combined with the cable terminal simulation model, the load impedance of the middle branch end of the cable is randomly changed to 25-85Ω, and a total of 35 groups of channel frequency responses of localized thermally aging cables under different load conditions are obtained. Figure 7 shows the channel frequency response of one group of localized thermal aging cables. It can be seen from the channel frequency response of the localized heat aging cable that when the cable leaks due to local aging and other problems, the temperature of the part rises continuously, resulting in the maximum temperature of the localized and the overall temperature rises to the point of damaging the cable and affecting the operation of the system, which results in the channel response being less than 0 dB, i.e., not responding normally, no matter what frequency is used. Combined with the results of the cable thermal characteristics test, when there is localized thermal aging of the cable, maintenance and replacement should be carried out in a timely manner to avoid the situation where the channel frequency cannot respond.

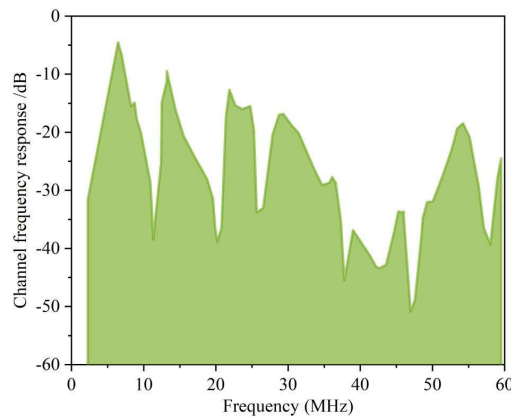


Figure 7: Channel Frequency Response of Local Thermally Aged Cables

## IV. Conclusion

In this paper, SSA-SVM model and thermal imaging technology are used comprehensively to realize the effective detection of cable thermal characteristics. The temperature of the cable strip rises to 65.43°C as the cable length increases from 0 to 60m, and the temperature peaks at 25m and 45m, which generate localized hot spots. The maximum temperature of the cable strip shows a trend of rapid decrease (73°C down to 66°C) and then stabilization (65°C) with increasing mass flow rate. The thermal gradient entropy yield showed a decreasing law with the increase of coolant mass flow rate. The final detection and analysis of the thermal characteristics obtained: cable local thermal aging, can not continue to respond to the electrical signal, the channel frequency response is always less than 0 dB. The use of this paper's technology for the thermal characterization of the cable, you can find the temperature anomaly of the cable law. In the future, the detection speed of the detection technology can be continuously improved to achieve rapid troubleshooting of cable faults.

## Funding

This work was supported by Technology project of funded by State Grid Hebei Electric Power Co., Ltd. (Grant number: KJ2022-016).

## References

- [1] Xia, C., Ren, M., Wang, B., Dong, M., Xu, G., Xie, J., & Zhang, C. (2021). Infrared thermography-based diagnostics on power equipment: state-of-the-art. *High Voltage*, 6(3), 387-407.
- [2] Xie, Y., Zhao, Y., Bao, S., Wang, P., Huang, J., Liu, G., ... & Li, L. (2020). Rejuvenation of retired power cables by heat treatment: experimental simulation in lab. *IEEE Access*, 8, 5635-5643.
- [3] Li, S., Cao, B., Li, J., Cui, Y., Kang, Y., & Wu, G. (2023). Review of condition monitoring and defect inspection methods for composited cable terminals. *High Voltage*, 8(3), 431-444.
- [4] Alboyaci, B., Cinar, M. A., Demiroglu, Y. B., & Ince, A. (2022). Evaluation of the effect of structural defects in the heat-shrink cable terminal on electric field distribution. *Engineering Failure Analysis*, 132, 105920.
- [5] Li, X., Du, L., Hu, Y., Xie, H., & Luo, L. (2024). Analysis of heating defects in extension rods of extra-high voltage direct current overhead transmission lines. *Electric Power Systems Research*, 233, 110507.
- [6] Xie, Q., Chen, H., & Yuan, Y. (2020). Heat blockage of air gap for inner overheating of high-voltage power cable and delay of early detection. *Journal of fire sciences*, 38(4), 363-376.
- [7] Zhang, L., LuoYang, X., Le, Y., Yang, F., Gan, C., & Zhang, Y. (2018). A thermal probability density-based method to detect the internal defects of power cable joints. *Energies*, 11(7), 1674.
- [8] Li, Z. (2024). Analysis of internal defects in power cables based on temperature field simulation. *Advances in Engineering Innovation*, 10, 36-48.
- [9] Li, Z., Zhou, K., Xu, X., Meng, P., Fu, Y., & Zeng, Z. (2023). A thermal excitation based partial discharge detection method for cable accessory. *IEEE Transactions on Power Delivery*, 38(4), 2703-2710.
- [10] Xu, Z., Zhu, D., & Zhang, Z. A. (2024). Research on Electrical Equipment Overheating Fault Identification Based on Infrared Technology. In *Intelligent Computing Technology and Automation* (pp. 121-129). IOS Press.
- [11] Mu, L., Xu, X., Xia, Z., Yang, B., Guo, H., Zhou, W., & Zhou, C. (2021). Autonomous analysis of infrared images for condition diagnosis of HV cable accessories. *Energies*, 14(14), 4316.
- [12] Shi, Z., Zhao, Y., Liu, Z., Zhang, Y., & Ma, L. (2021). Diagnosis and classification decision analysis of overheating defects of substation equipment based on infrared detection technology. *Scientific Programming*, 2021(1), 3356044.
- [13] Zheng, Y., & Sun, B. (2023, May). Power cable terminal fault detection method based on infrared thermal imaging. In *Journal of Physics: Conference Series* (Vol. 2503, No. 1, p. 012040). IOP Publishing.
- [14] XIA, Z., YANG, B., GUO, H., XU, X., ZHOU, W., & ZHOU, C. (2022). Extraction method of overheating regions in infrared images of cable terminations. *Journal of Electric Power Science and Technology*, 37(2), 12-21.
- [15] Liang, H., Li, Z., Liu, Z., Li, Q., Zhang, S., Zhang, Z., ... & Zhou, C. (2025). Infrared image-based multi-point temperature monitoring for ultra-high-voltage direct current wall bushings subject to insulation shed interference. *High Voltage*.
- [16] dit Leksir, Y. L., Mansour, M., & Moussaoui, A. (2018). Localization of thermal anomalies in electrical equipment using Infrared Thermography and support vector machine. *Infrared Physics & Technology*, 89, 120-128.
- [17] Liu, G., Wen, Y., Gu, Y., Zhou, J., & Chen, S. (2025). Decision Tree Clusters: Non-destructive detection of overheating defects in porcelain insulators using quantitative thermal imaging techniques. *Measurement*, 241, 115723.
- [18] Ullah, I., Yang, F., Khan, R., Liu, L., Yang, H., Gao, B., & Sun, K. (2017). Predictive maintenance of power substation equipment by infrared thermography using a machine-learning approach. *Energies*, 10(12), 1987.